CONTRIBUTIONS TO THE STUDY OF MECHANICAL AND CAVITATIONAL BEHAVIORS OF THE MAGNESIUM ALLOY TYPE AM50

Liviu Daniel PIRVULESCU[1], Ilare BORDEASU [2,3] *, Brandusa GHIBAN[4*]

The use of magnesium-based alloys has gained momentum in the manufacture of components in fields such as automotive, aerospace, medical, military, etc., due to their low specific mass, around 1.7 g/cm3, but also to their pressure casting capacity, obtaining parts of superior geometric quality, with physical-mechanical properties and homogeneous microstructure in the volume of the parts. At the same time, recent research aims to expand their application in the biomedical field for reparative surgery. In line with new research, the paper presents the results obtained in the cavitation testing of the magnesium-based alloy AM50, with the aim of its use in cardiac devices that work in hydrodynamic conditions, such as stents. The evaluation of the behavior and resistance performances is made by comparing them with those of the ZnMg and ZnMgFe alloys, whose resistance performances to cyclic cavitation stresses are studied and known. holding times, brings new elements, compared to those already obtained on the same brand of alloy and with the same heat treatment regime. The results presented are of real use to those who design and build equipment with structures from this alloy and who work in a non-stationary, cavitational hydrodynamic regime.

Keywords: magnesium alloy, mechanical properties, cavitation erosion resistance, stereomicroscopy, biomedical application

1. Introduction

The widespread use of magnesium-based alloys has been avoided for many years due to magnesium's high cost, low resistance to corrosion, high flammability and self-explosion. As a result of the excellent strength-to-weight ratio and the ability to obtain lightweight, dimensionally accurate and complex geometry parts through pressure casting, extensive research has led to the creation of magnesium-based alloys that are now widely used in the automotive, aerospace, medical,

[1] Assoc. Professor, Dept. of Mechanics and Strength of Materials, University POLITEHNICA of Timisoara, Romania, liviu-daniel.pirvulescu@upt.ro

[2] Professor, Dept. of Mechanical Machines Equipment and Transportation, University POLITEHNICA of Timisoara, Romania, corresponding author, Corresponding author: e-mail: ilarica59@gmail.com

[3] Professor, Romanian Academy of Scientists, Timisoara branch, Romania, ilarica59@gmail.com

[4] Dept. of Metallic Materials Science and Physical Metallurgy Department, National University of Science and Technology POLITEHNICA Bucharest, Romania, corresponding author, e-mail: brandusa.ghiban@upb.ro

military and other industries, where their high cost (some grades contain quite expensive alloying elements) is economically justified by the possibility of creating lighter, more durable, faster, stronger and safer equipment that can operate efficiently under extreme conditions, including when exposed to high temperatures [1, 2]. This category also includes the AM50 alloy, whose use in the automotive field is certified by the advantages it brings. Due to its biodegradability and biocompatibility, new research [3-6] are oriented towards the use of magnesium-based alloys in the biomedical field, in orthopedic surgery (in various prostheses) and cardiovascular surgery (in stents and heart valves), such as those based on zinc [7-12]. For this purpose, simulations are carried out with specialized software [13-19] on the analysis of factors that influence the behavior of materials under mechanical and hydrodynamic loads. The analysis of the behavior under hydrodynamic loads is necessary because the circulatory system is known to be a hydraulic network in which the heart plays the role of a pump, and the veins and arteries as hydraulic pipes. As a result, studies carried out on hydraulic networks, through various simulations [15-19] and laboratory research [19-24], require knowledge of the behavior of biocompatible alloys used in reparative surgery under mechanical and hydrodynamic stress. Since the behavior of the AM 50 alloy under mechanical stress, to which the components of the vehicle structure are subjected, is being investigated [1-6, 25, 26], for its use in prosthetic devices and devices in cardiac surgery, it is necessary to know the behavior under the stresses generated by the hydrodynamics of blood flow. The aim of the current study is to investigate the mechanical and hydrodynamic response of the AM50 alloy in its cast semi-finished state when subjected to microjets and shock waves generated by the implosion of cavitation bubbles induced by blood flow dynamics.

2. Researched material and investigation methods

The investigated material is a magnesium alloy type AM50, whose chemical composition is shown in Table 1. The chemical composition was determined with an optical emission spectrometer (Thermo Electron ARL 3460) and the alloy was obtained by pressure casting.

Table 1.

Chemical composition of the investigated Mg alloy (in %) [1]

Material	Al	Mn	Zn	Fe	Ni	Cu	Si	Be	Mg	Other
AM50	4.70	0.32	0.13	0.002	0.001	0.004	0.03	0.0014	94.77	0.005

Structural analyses were performed on the experimental alloy, as well as determinations of the mechanical behavior under repeated shocks and cavitation behavior.

2.1 Equipment used for structural and fractographic characterization

Microstructural analysis was performed in the Physical Metallurgy laboratory at National University of Science and Technology POLITEHNICA Bucharest, using an OLYMPUS metallographic microscope equipped with image processing software. Fractographic analysis was performed on an OLYMPUS SYL stereomicroscope, equipped with QUICKmicroPHOTO 2.2 software.

2.2 Apparatus used in mechanical experiments

Repeated impacts define the fatigue phenomenon, known as impact fatigue [1], identical to that between a shock wave surface and the microjets resulting from the implosion of cavitation bubbles. This research is necessary because the strain rate modifies the characteristics of the material and, as a consequence, it is expected that the material properties will be different from those obtained in non-impact fatigue.

In general, an impact occurs as a consequence of the collision between two bodies (hammer-specimen), the impact force being accompanied by the transmission and reflection of stress waves that begin at the point of contact and are influenced by the shape and dimensions of the specimens and the loading conditions.

For the repeated impact test, Charpy V-notch specimens were used, according to SR EN ISO 148-1:2017, Fig. 1.

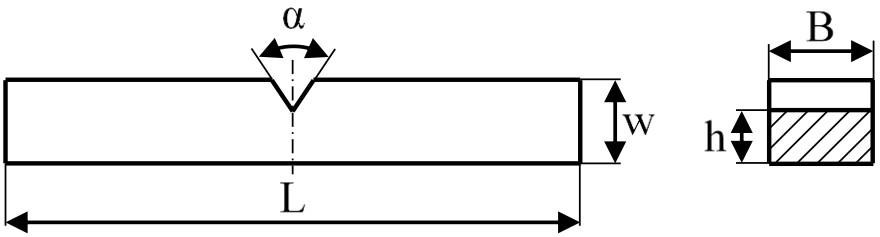

Fig. 1. Charpy V-notch specimens for repeated impact testing

The dimensions of the experimental specimens have the values presented in Table 2. The radius at the base of the notch has a nominal size of 0.25 mm and a machining tolerance of ± 0.025 mm.

Table 2.

Specified dimensions and tolerances of the Charpy V-notch specimen

Name	**Symbol**	**Nominal size [mm]**	**Machining tolerance [mm]**
Length	**L**	55	± 0.60mm
width	**W**	10	± 0.075mm
depth	**B**	10	± 0.11mm
Notch angle	**α**	45°	± 2°
ligament	**h**	8	± 0.075mm

Testing of mechanical behavior under repeated shocks was done in the specialized laboratory of Politehnica University of Timisoara. For testing, the specimens were simply supported at both. A very important aspect of repeated impact testing is that the impact hammer strikes the specimen centrically on the opposite side of the notch, in the same place with each blow. For testing, the specimens were simply supported at both.

A force transducer was mounted on the impact hammer, which performs the repeated impact, to measure the maximum force with which it strikes. Before performing the mechanical tests, the force transducer was calibrated on the tensile/compression testing machine.

The test was carried out in the Materials Strength Laboratory of the Politehnica University of Timisoara on the Amstel type repeated impact testing machine, adapted for repeated impact bending tests. The testing machine is equipped with a cycle counter that indicates the number of blows applied to the specimen until breakage.

In Table 3 the average values of the mechanical properties at tensile and their dispersion are shown, determined and analyzed by Marșavina & ao [1].

Table 3

Tensile strength properties of the investigated Mg alloy [1].

Material	Modulus of elasticity MPa	Tensile strength, R_m MPa	Yield strength, $R_{p0.2}$ MPa	Deformation at break %
AM 50 from tests	45870 ± 1450	236.9 ± 10.5	122.8 ± 1.4	14.5 ± 1.8

2.3 Equipment used in cavitation tests

Cavitation testing aims to highlight the behavior and resistance of the AM 50 alloy structure to cyclic cavitation stresses which, through impact forces, produce deformations and microcavities that transform the cavitated surface into a sponge-like one with a certain porosity. The cavitation behavior and resistance test was carried out on 3 samples, on the vibrating device with piezoceramic crystals, in the Cavitation Erosion Research Laboratory of the Polytechnic University of Timisoara [22].

The tests were carried outin distilled water by the indirect method (with stationary sample [7-11, 27-29]). The testing procedure and the division of the total duration of 165 minutes into intermediate periods, at the end of which mass losses were measured and eroded surfaces were photographed, followed the steps specific to laboratory custom [22], in compliance with the requirements set out in ASTM G32-2016 standards [30]. Before starting the test, the surface exposed to cavitation was polished. The average roughness of 0.4 μm was measured with the Mitutoyo SJ 210 device.

The functional parameters of the device, which dictated the erosive intensity of the vibrating cavitation, were controlled and maintained at the values recommended by ASTM G32-2016 standards throughout the testing, thanks to the software implemented in the computer with which the experimental program was conducted [22, 31].

3. Experimental results and their interpretation

3.1. Microstructural analysis

Metallographic appearance of the experimental alloy AM50 is illustrated in Fig. 2. This analysis was determined in the Laboratory of the Special Materials Expertise Center of the National University of Science and Technology Politehnica Bucharest. The image shows a microstructure formed by solid solution α, solid solution β-$Mg_{17}Al_{12}$ and brittle intermetallic compounds AlMn [32].

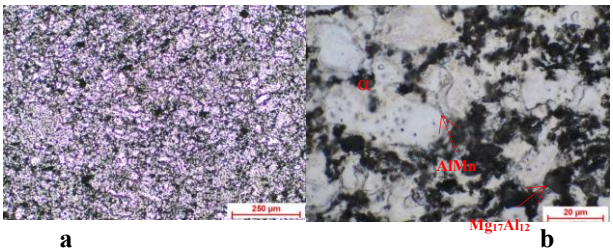

a **b**

Fig. 2-Microstructural appearance of the experimental alloy AM50 (6% nital attack): A-x 100; b- x500

3.2. Repeated shock test results

During the repeated shock test, the maximum impact force and the number of blows until the specimen failed were determined.

For each specimen, the dimensions were measured using an electronic caliper with a precision of 0.01 mm, and then the net cross-sectional area was determined. The results obtained are presented in Table 4.

Table 4.

Dimensions and net area of test specimens

Specimen	Specimen dimensions [mm]				Net area [mm^2]
	Length L	Width W	Thickness B	Ligament h	
1	75.18	9.90	9.90	8.53	84.45
2	75.20	9.98	10.02	8.52	85.37
3	75.32	9.86	9.92	8.50	84.32
4	75.38	9.98	10.07	8.52	85.80
5	75.35	9.42	9.99	8.52	85.11

Knowing the dimensions of the specimen, the modulus of resistance of the cross-section of the specimen was determined (M_zW_z), and based on the maximum force, the maximum bending moment was determined ($M_{iz,max}M_{iz,max}$) and the maximum voltage (σ_{max}) upon impact of the specimen subjected to three-point bending. The following relations were used to calculate the above quantities:

$$W_Z = \frac{b \cdot h^2}{6}; \quad M_{iZ,max} = \frac{F_{max} \cdot L}{4}; \quad \sigma_{max} = \frac{M_{iZ,max}}{W_z} \tag{1}$$

After performing repeated shock tests, based on the above relationships and the geometric dimensions of the 5 tested specimens, the obtained results were presented in Table 5.

In Fig. 3 the dependence between the number of blows and the maximum stress applied to the specimen, obtained from repeated impact tests, is presented. A relatively small dispersion (scattering) of the data regarding the number of blows is observed for all the tested specimens. The differences that appear between the maximum impact forces for the 5 specimens are determined by the difference in thickness between the specimens and the way the striker is detached from the cam. It is observed that the specimens with the lowest number of blows (specimens 1 and 3) have the smallest net area and the lowest modulus of resistance, which leads to the lowest stresses.

Table 5.

Results obtained after testing the specimens under repeated shocks

Specimen	Maximum force F_{max} kN	The modulus of resistance W_z mm^3	Bending moment $M_{iz,max}$ N·mm	Maximum stress, σ_{max} MPa	Number of strokes
1	4.503	120.06	84633.89	704.961	191
2	4.859	121.23	91349.20	753.548	318
3	4.402	119.45	82889.66	693.913	233
4	4.564	121.83	86008.58	705.970	300
5	4.663	120.86	87839.26	726.776	326

When the modulus of resistance has higher values (specimens 2 and 5 - see also Table 5) an increase in both the maximum stress (over 720 MPa) and the number of blows (over 320) until the specimens break is observed.

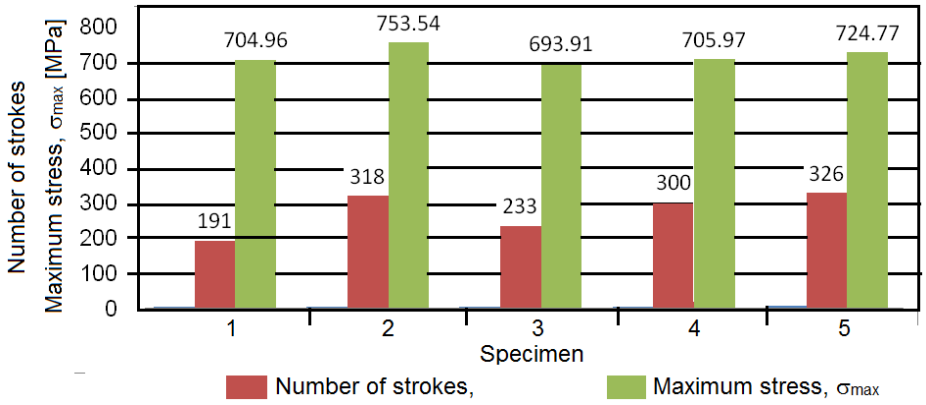

Fig. 3 Comparison between the number of blows and the tension applied to the specimens

It should be noted that, in the case of the present study, the higher the stress concentration factor (V-notch geometry), the lower the stress of the specimen and obviously the lower the number of blows that the V-notch specimen can withstand. Thus, referring to the number of blows of 326 (sample 5), for which the maximum stress is 726.77 MPa, by decreasing the number of blows by 135 (sample 1-191 blows), the maximum stress decreases by about 3% (704.96 MPa). This comparison

shows that the presence of a defect in the stressed structure decreases its resistance to the number of blows.

This evaluation justifies the negative effect of a defect not only on the mechanical resistance to fracture, but also on the resistance of the structure to cyclic cavitation stresses, as will be seen in the chapter with the cavitation test results. The macroscopic appearance of the V-notched resilience specimens is shown in Fig. 4. In longitudinal section (fig.6a,b) the propagation of the fracture front is observed to be approximately linear, in the same plane, and in transverse section (fig.6c,d) the presence of a fibrous structure, with parallel wrinkles is noted. Upon detailed analysis, the propagation of the front is evident to be intergranular, with the formation of secondary cracks and unevenness of over 1mm depth.

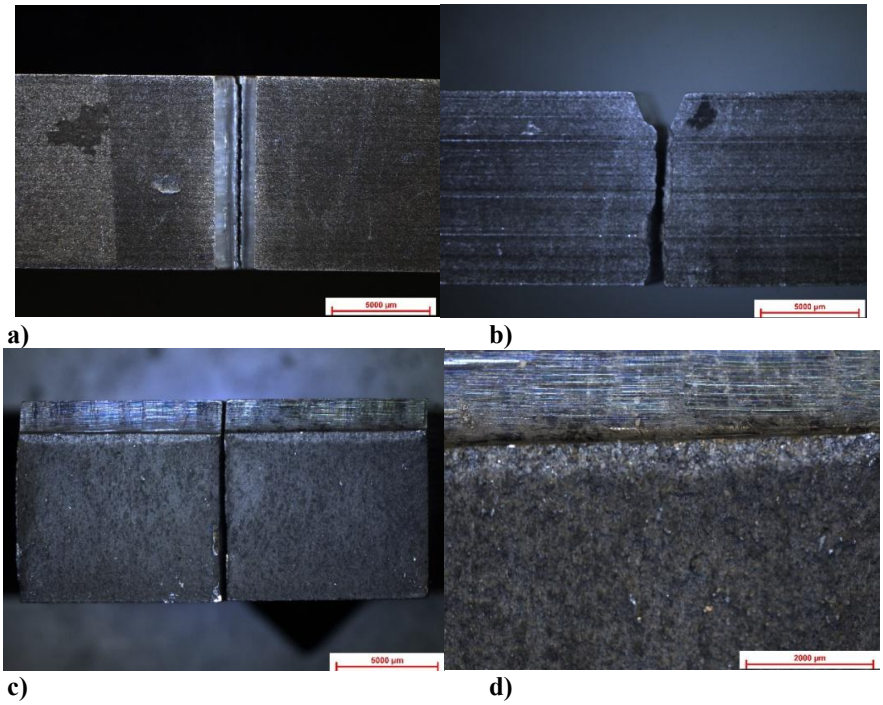

Fig. 4 Macroscopic appearance of V-notch resilience specimens:
a,b - longitudinal section; c, d - transverse section

3.3 Results of the test after cavitation

The results of the cavitation test are presented through specific diagrams and macro and microstructural images that allow morphological analysis of the destruction of the structure through the erosion effect.

a) Specific curves and parameters

The diagrams that serve to analyze the behavior and resistance of the surface structure to the stresses of shock waves and cavitational microjets are presented in

Fig.5 and contain the evolutions of the mean penetration depth MDE(t) and the mean erosion penetration rate MDER(t) with the duration of the cavitation attack.

The experimental values of the three samples, determined according to the mass losses with relations (2) and (3), are expressed by the pink, green and black dots.

$$MDEi = \sum_{i=1}^{i=12} \frac{4 \cdot \Delta M_i}{\rho \cdot \pi \cdot d_p^2} \quad [\mu[m] \tag{2}$$

$$MDERi = \frac{4 \cdot \Delta M_i}{\rho \cdot \pi \cdot d_p^2 \cdot \Delta t_i} [\mu m/min] \tag{3}$$

Where:

ΔMi – is the mass loss obtained at the end of each intermediate test period, following weighing with the Kern 101BT-5NM analytical balance

i – the number of the intermediate period

Δti – duration of the intermediate period (first 5 min, second 10 min, the rest 15 min each)

dp = 15.8 mm – diameter of the surface exposed to cavitation

The averaging of the valueswas done through curves whose analytical forms are determined with the relationships established by Bordeasu & collaborators [22, 32], whose analytical form and coefficient values are displayed inside the diagrams.

The legends of the diagrams provide information about the accuracy of the experiment and about the values of the parameters MDE_{max} and $MDER_s$ that are the basis for evaluating the strength of the cavity structure. To express the accuracy of the experiment, the dispersion range of the experimental values is delimited by the tolerance interval (dispersion) curves, S98(t) and I98(t), corresponding to the average standard deviation σ = 0.283 and the approximation error of the experimental values by the MDER(t) curve, $\varepsilon = \pm 2\%$.

His valuesσandεshows that the testing of the three samples was carried out under identical conditions, in which the functional parameters of the device were very well controlled and maintained at the prescribed values (vibration amplitude = 50 μm, vibration frequency 20 ± 0.1 kHz, power of electronic ultrasound generator = 500 W, water temperature 22 ± 1^0C). Also, the values of the statistical parametersσandεshows that the mechanical properties of the three samples (especially hardness) are of the same order in the volumes and surfaces of the three samples.

From the point of view of the behavior of the alloy structure to cyclic cavitation stresses, the analysis of the dispersions of the experimental values and the shape of the evolution of the averaging curves from Fig.5, we find:

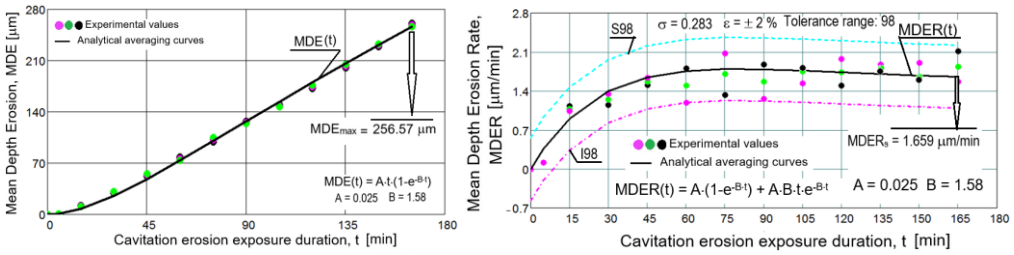

a) b)

Fig. 5 Specific diagrams of cavitation erosion behavior: a - variation of average erosion depth with cavitation attack duration; b - variation of average erosion velocity with duration of cavitation attack

- low resistance to the forces developed by the impact of the surface with shock waves and cavitational microjets, in the first part (0...(30) 45 minutes), reflected by the exponential increase in the cumulative losses and the MDE(t) curve and the increase towards a maximum in the erosion rates, respectively the MDER(t) curve. This behavior also shows the detrimental effect of the degradation of the magnesium-based alloy in an aqueous environment;

- mechanical hardening of the cavity surface under cyclic cavitation stresses, reflected by the relative stabilization of erosion rates and mass losses in the intermediate intervals after the 45 minutes, as well as by the linear evolution of the MDE(t) curve up to the maximum value MDE_{max} = 256.57 µm and with a slight asymptotic decrease of the MDER(t) curve towards the final stabilization value $MDER_s$ = 1.659 µm/min;

- the differences between the experimental values of the three samples are reduced. This behavior, according to previous studies [20, 21]. It is also caused by the damping effect of air and water, from the microcavities formed, on the impact force of the microjet or shock wave, in addition to the increase in hardness mentioned above.

b) Morphology of structural degradation

A first assessment of the morphology of the surface structure degradation, through the erosion of vibratory cavitation, is made based on photographic images from Fig. 6 (taken with the Canon Power Shot A 480 camera) from 3 significant durations of the cavitation attack and the microscopic ones from Fig. 7 and Fig. 8. From these images it can be observed the poor resistance of the structure, due to the degradation in the liquid test environment, highlighted by the difference between the surface appearance before the cavitation attack (minute 0), which is smooth and finished to a roughness Ra = 0.4 µm, the one at minute 1 (one), in which the surface has plastic deformations, networks of cracks and microcavities and the one at the end of the 165 minute attack when the surface is full of caverns.

0 minutes 1 minute 165 minutes

Fig. 6 Macro images of erosion evolution in the cavitated surface

The appearance of these microcavities, from the point of view of cavitation erosion mechanics, leads to the idea that their formation, in such a short time, is the effect of the expulsion of grains of fragile intermetallic compounds, highlighted by the microscopic image in Fig.2.

As can be seen, increasing the duration of cavitation exposure causes the multiplication of microcavities, simultaneously with an increase in the spreading area. This evolution is justified because, by increasing the duration of stress, the formed microcavities become crack initiators, contributing to the weakening of the bonding forces between the grains, whether they are of the base metal or of the ductile intermetallic compounds.

Also, the small difference between the surface aspects at 105 minutes and 165 minutes is noted. This closeness between the surface aspects at the two times is the effect of the mechanical hardening of the stressed structure and the damping of the impact pressure peaks, generated by the air and water penetrated into the formed microcavities and justifies the linear evolution of the MDE(t) curve in Fig. 5a and asymptotic decrease of the MDER(t) curve from Fig. 5b.

On the other hand, the very porous appearance of the cavity surface, with aThe multitude of caverns confirms not only the destructive force of cavitation but also the effect of its degradation in aqueous environments, which is accelerated by the repeated strikes of the surface with the high-speed water microjet which, in turn, is also aqueous in nature, being formed from the vapors contained in the cavitation bubble, through the implosion of which it was generated.

Therefore, to reduce the degree of cavitation damage, respectively to increase the resistance of the alloy structure to cavitation stresses, new research is needed to identify technologies that can reduce the degree of degradation in aqueous environments, in order to increase its resistance to cavitation erosion.

Fractographic analysis of the surfaces subjected to cavitation (both after 1 minute and after the completion of the test) shows that the implosion of the bubbles collapsing on it caused the initiation of pitting phenomena from the start phase of the attack, Fig.7 and Fig.8. Fractographic analysis shows that the mechanisms of material expulsion, during cavitation erosion, are determined by plastic and brittle

deformation processes, accompanied by the formation of slip steps. From the analysis of the appearance of the cavity surface it can be seen that, as a result of the increase in the number of collapses of the cavitation bubbles, the number of pinches that undergo the phenomenon of coalescence with the formation of fatigue microcracks increases.

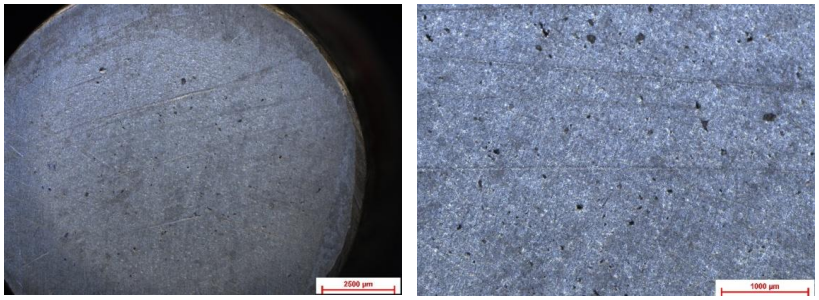

Fig. 7 Macroscopic appearance of AM50 alloy after 1 minute cavitation testing

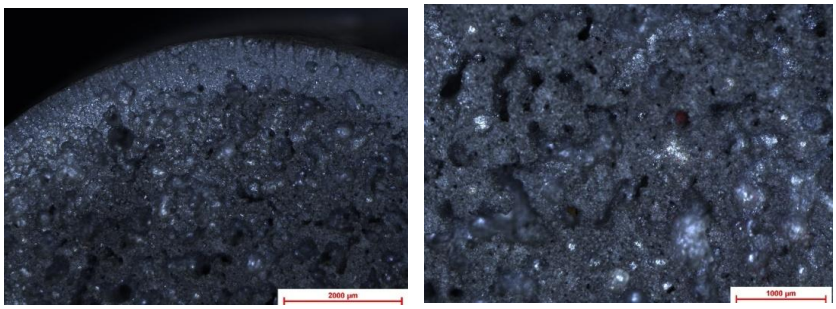

Fig. 8 Macroscopic appearance of AM50 alloy after cavitation testing for 165 minutes

In addition to these microcracks, generated on the interface between the microstructural phases (base material and brittle intermetallic compounds), a brittle removal of the matrix material is observed. The boundaries between the grains of the base metal are attacked by microcracking followed by the expulsion of some of them. The topographic image of the surface highlights the formation of craters whose depths are of various sizes (large and small), determined by the preferential cavities of the grain boundaries and of the boundaries between the brittle intermetallic phases and the base metal matrix, which are more fragile. We appreciate that these boundaries are not able to absorb the deformation energy due to the specific degradation in water and the stresses induced in the material by the cavitation impact waves and, as a consequence, the microstructure erodes very quickly.

c) Evaluation of the structure's resistance to erosive cavitation stress

For the analysis of the strength of the AM50 alloy structure, the values of the reference parameters for cavitation resistance are used.(MDE_{max} = 256.67 μm

and $R_{cav} = 1/MDER_s = 0.6$ min/μm) and macro and microscopic images from Fig.6, Fig. 7 and Fig. 8 Compared to other biodegradable alloys, such as zinc alloys [10] (ZnMg alloy: $MDE_{max} = 30.69$ μm, $R_{cav} = 4.97$ min/μm and ZnMgFe alloy: $MDE_{max} = 12.65$ μm, $R_{cav} = 10.31$ min/μm),it can be seen that the AM50 alloy has very poor cavitation resistance from 8 times to over 20 times lower. Analyzing the mechanical property values in Table 3, compared to the mentioned zinc-based alloys (see Table 6) we find that they are much lower: the mechanical strength at break σ_m from 2 to 2.8 times and the yield strength $\sigma_{p0.2}$ from 4.0 to 4.6 times.

Table 6.

The values of the mechanical properties of the zinc alloys

Alloy	R_m **[MPa]**	$R_{p0.2}$ **[MPa]**	**Hardness HB [daN/mm²]**	A_5 **[%]**	**E [MPa]**
ZnMg	85	26.61	48	2.66	1.39
ZnMgFe	108	30.7	74	3.69	8.09

Therefore, the question arises how to explain the poor resistance when studies conducted on ferrous alloys (steels, cast irons) and non-ferrous alloys (brass, bronzes, aluminum and zinc-based alloys, composite materials) [8-11, 21, 29, 31, 33 - 37] shows that, in general, the cavitation resistance of a material structure increases with increasing mechanical properties? The explanation of the poor resistance of the AM50 alloy, in relation to other zinc-based alloys (ZnMg and ZnMgFe), despite higher values of its mechanical properties, is given by the effect of its high degradation in aqueous environments. Therefore, as previously stated, the multitude of caverns is also explained by the decrease in the resistance of the structure to the impact forces produced by the high-speed water microjet and the shock wave, which are also of an aqueous nature.

Considering the objective pursued, that of creating cardiac devices (stents and valves), which work in the blood circulatory system, with physical characteristics completely different from those of water, it is expected that, in this case, its resistance will be completely different from that presented in the work and the high effect of the mechanical properties will be felt in a positive sense.

4. Conclusions

The following conclusions could be made after the investigation of the structural, mechanical and cavitation erosion behaviour of magnesium alloy type AM50:

1. The microstructure of the experimental magnesium alloy AM50 consists of a magnesium-based solid solution α, solid solution β-$Mg_{17}Al_{12}$ and brittle intermetallic compounds AlMn with a uniform arrangement in the metal matrix;

2. The V-notch, as a stress concentrator factor, causes fatigue life to decrease through repeated impacts.
3. Small dispersion of the number of blows, for all tested specimens, and the differences between the number of blows are due to the thickness of the specimens, the force of the impact hammer and the arrangement of brittle intermetallic compounds in the solid solution in the alloy microstructure.
4. The macrostructural appearance of V-notched impact specimens is that of a fibrous structure, with intergranular propagation of the fracture and the formation of secondary cracks in the matrix, as the fracture front propagates.
5. The poor resistance of the AM 50 alloy structure to cavitation generated in water is determined by its high degree of degradation in aqueous liquid environments, the influence of the mechanical property values being insignificant.
6. From the point of view of the mechanical aspect of behavior under cavitation stresses, the structure follows the specific mechanism of increasing losses on the first part of the attack (when the cumulative losses increase exponentially and the erosion rates increase towards a maximum) and of stabilization on the second part (when the losses are relatively constant, determining the linearization of the cumulative loss averaging curve MDE(t), respectively the decrease towards the stabilization value of the erosion rate averaging curve MDER(t)).
7. Although the alloy degrades in the liquid medium used, as the cavitation duration increases, the attacked surface layer mechanically hardens, and the microcavities formed contribute to the damping of impact pressure peaks through the air and water that penetrates them, reducing losses during intermediate durations.
8. The accentuation of the degradation of the cavity surface, by multiplying the number of microcavities, despite the values of the mechanical properties, is also determined by the aqueous character of the cavitational waves and microjets, beyond the amplitude of the stresses induced by their impact with the surface exposed to the attack.
9. To increase the resistance to cavitation in aqueous environments of the AM 50 alloy, it is necessary to use traditional or new technologies to reduce its degradation capacity.
10. It is necessary to test the alloy in a liquid environment with physico-chemical characteristics in which the resistance of the AM 50 alloy to erosive cavitation stresses is no longer influenced by its degradation property as in aqueous environments.

REFERENCES

[1] *L. Marsavina, F. Iacoviello, LD Pîrvulescu, V. Di Cocco, L. Rusu,* Engineering prediction of fatigue strength for AM50 magnesium alloys, International Journal of Fatigue, **127**, pp. 10-15, 2019

[2] ***https://aludiecasting.com/ro/proprietati-ale-aliajului-de-magneziu-turnat-sub-presiune-az91d/
[3] *G.L. Dragomir*, Mg-Zn-Ag Alloys for Orthopedic Implants, PhD thesis, UP Bucharest, Romania, 2023.
[4] *V. Manescu, I. Antoniac, A. Antoniac, D. Laptoiu, G. Paltanea, R. Ciocoiu*, Bone Regeneration Induced by Patient-Adapted Mg Alloy-Based Scaffolds for Bone Defects: Present and Future Perspectives, Biomimetics, **8** (8), 618, 2023.
[5] *S. Zhang, X. Zhang, C. Zhao, J. Li, Y. Song, C. Xie, H. Tao, Y. Zhang, Y. He, Y. Jiang, Y. Bian*, Research on an Mg–Zn alloy as a degradable biomaterial, Acta Biomater., **6**(2), pp. 626-640, 2010.
[6] *I. Antoniac, M. Miculescu, V. Mănescu, A. Stere, PH Quan, G. Paltanea, A. Robu, K. Earar,* Magnesium-Based Alloys Used in Orthopedic Surgery. Materials, **15**, 1148, 2022.
[7] *I. Bordeasu, C. Ghera, AN. Luca, A. Manea, DC. Stroita, L.C. Salcianu, B. Ghiban, L.M. Micu*, Investigation of Cavitation Resistance of Biocompatible Zinc-Based Alloys for Biomedical Applications, International Conference on Machine and Industrial Design in Mechanical Engineering, 272-281, 2024.
[8] *G. Ciungu, L.M. Micu, I. Bordeasu, C.M. Iordache, B. Ghiban, C. Ghera,* Research of the Cavitation Resistance of a Biodegradable Zn-Cu Alloy, UPB Sci. Bull. Series B, 86(3), 2024.
[9] *C.M. Iordache, A.N. Luca, I. Bordeasu, G. Ciungu, B. Ghiban,* Cavitational Erosion Behavior of a Biodegradable Alloy from the Zn-Mg System for Biomedical Applications.Tribol. Ind., **46**, pp.315–323, 2024.
[10] *C.M. Iordache (Gheorghe),* Correlation between structure-mechanical characteristics-biodegradability-cavitation of some biomedical alloys form the system ZnMg(Fe), PhD Thesis, National University of Science and Technology Politehnica Bucharest, 2024 (in Romanian)
[11] *G. Ciungu*, Experimental Studies on the Cavitation and Biodegradation Behavior of Some Alloys of the System ZnCu(Mg) System.PhD Thesis, University Politehnica Bucharest, Bucharest, Romanian, 2024.
[12] *I. Bordeasu, C. Ghera, A.N. Luca, A.S. Manea, D.C. Stroita, C.L. Salcianu, B. Ghiban, L.M. Micu,* Investigation of Cavitation Resistance of Biocompatible Zinc-Based Alloys for Biomedical Applications, International Conference on Machine and Industrial Design in Mechanical Engineering, pp.272-281, 2025.
[13] *R. Cormos, H. Petrescu, A. Hadar, H. George,* Finite Element Analysis of the Multilayered Honeycomb Composite Material Subjected to Impact Loading, Mat.Plast. **54**(1), pp. 180-185, 2017.
[14] *A. George, A.Z. Apostolescu, C.G Amza, L. Anton,* Determination through numerical computation of the designed and functional parameters of ultraacoustic systems for ultrasonic welding of intelligent composite materials, 2007, Mat.Plast. **44** (2), 2007, 121-128.
[15] *D. Bordeasu, F. Dragan, I. Filip, I. Szeidert, G.O. Tirian*, Estimation of Centrifugal Pump Efficiency at Variable Frequency for Irrigation Systems, Sustainability, Vol. **16**, Iss. 10, 2024.
[16] *D. Bordeasu*, Study on the implementation of an alternative solution to the current irrigation system, Acta Technica Napocensis-Series: Applied Mathematics, Mechanics, And Engineering, Vol. **65**, no.3s, 2022.
[17] *A.A. Anton,* A method for describing computational science, Annals of DAAAM & Proceedings, vol.**20**, pp. 839-840, 2009.
[18] *F. Dragan, D. Bordeasu, I. Filip*, Determining the Operating Performance of an Isolated, High-Power, Photovoltaic Pumping System Through Sensor Measurements, Applied Sciences, **15** (15), 8639, 2025
[19] *D.C. Stroita, D. Bordeasu, F. Dragan,* System Identification of a Servo-Valve Controlled Hydraulic Cylinder Operating Under Variable Load, Mathematics, **13** (3), 341, 2025.
[20] *J.P. Franc, J.L. Kueny, A. Karimi, D.H. Fruman, D. Fréchou, L. Briançon-Marjollet. J.Y. Yves Billard, B. Belahadji, F. Avellan, J.M. Michel,* La cavitation. Mécanismes physiques et aspects industriels , Press Universitaires de Grenoble, Grenoble, France, 1995.
[21] *R. Garcia, F.G. Hammitt, R.E. Nystrom,* Correlation of cavitation damage with other material and fluid properties, Erosion by Cavitation or Impingement, ASTM, STP 408 Atlantic City, USA, 1966.

[22] *I. Bordeasu*, Monograph of the Cavitation Erosion Research Laboratory of Politehnica University Timisoara (1960-2020), Politehnica Publishing House, Timişoara, Romania, 2020.
[23] *D.C. Stroita, A.S. Manea, A. Cernescu,* Blade polymeric material study of a cross-flow water turbine runner, Materiale Plastice, Vol. **56**, Iss. 2, pp. 366 –369, 2019, DOI: 10.37358/MP.19.2.5187.
[24] *D. Tokar, C. Stroita, A. Tokar, A. Rusen*, Hybrid System that integrates the Lost Energy Recovery on the Water-Water Heat Pump Exhaust Circuit, IOP Conference Series: Materials Science and Engineering, Vol. **603**, no. 4, 042002, 2019.
[25] *C.M. Sonsino, K. Dieterich*, Fatigue design with cast magnesium alloys under constant and variable amplitude loading. Int J Fatigue **28**, pp.183–93,2006;.
[26] *J. Dallmeier J, Denk J, Huber O, Saage H, K. Eigenfeld,* A phenomenological stress-strain model for wrought magnesium alloys under elastoplastic strain-controlled variable amplitude loading. Int J Fatigue**, 80**, pp.306–323, 2015.
[27] *D. Istrate*, Influence of heat treatments on the behavior of an alloy from the Al-Mg system for maritime applications, Doctoral thesis, UP Bucharest, Romania, 2023.
[28] *I. Bordeasu, I. Mitelea, L. Salcianu, C.M. Craciunescu,* Cavitation Erosion Mechanisms of Solution Treated X5CrNi18-10 Stainless Steels, Journal of Tribology-Transactions of the AEMS, **138** (3), 031102, 2016
[29] *I. Dionisie, C. Ghera, L. Sălcianu, I. Bordeaşu, B. Ghiban, D.V. Băzăvan, L.M. Micu, D.C. Stroiță, D. Ostoia*, Heat Treatment Influence of Alloy 5083 on Cavitational Erosion Resistance, Hydraulica, no. **3**, pp. 15-25, 2021
[30] *** ASTM, Standard G32; Standard Method of Vibratory Cavitation Erosion Test. ASTM: West Conshohocken, PE, USA, 2016.
[31] *O. Oanca*, Techniques for optimizing the resistance to cavitation erosion of CuAlNiFeMn alloys intended for the manufacture of naval propellers, Doctoral thesis, Timişoara, 2014.
[32] *I. Bordeasu, C. Patrascoiu, R. Badarau, L. Sucitu, M.O. Popoviciu, V. Balasoiu*, New contributions to cavitation erosion curves modeling, FME Transactions, **34**(1), pp.39-43, 2006
[33] *LE Anton, I. Bordeasu, I. Tabara,* Considerations regarding the use of EPO 99 B resin in manufacturing AXIAL hydraulic machinery runners, Mat. Plastic, **45(2)**, pp.190-192, 2008
[34] *P. Cheng-Cheng, X. Yes-Hai, H. Meng-Yang, Q. Zhenbo, X. Yunze, B. Yashar, H. Wenbin*, Cavitation erosion of the AA7050 aluminum alloy in 3.5 wt% NaCl solution—Part 1: mitigating effect by corrosion,Corrosion Science, vol.**232**, 112012, 2024.
[35] *J. Carlton,* Marine propellers and Propulsion, Elsevier Ltd: Oxford, Great Britain, 2007.
[36] *W.J. Tomlinson, S.J. Matthews*, Cavitation erosion of aluminum alloys, Journal of Materials Science, Vol. **29**, pp.1101-1108, 1994.
[37] *S. Vaidya, C.M. Preece,* Cavitation erosion of age-hardenable aluminum alloys, Vol. **9**, pp. 299–307, 1978.